ACS Catalysis

Research Article

pubs.acs.org/acscatalysis

Asymmetric Epoxidations with H_2O_2 on Fe and Mn Aminopyridine Catalysts: Probing the Nature of Active Species by Combined Electron Paramagnetic Resonance and Enantioselectivity Study

Oleg Y. Lyakin,[†] Roman V. Ottenbacher,[‡] Konstantin P. Bryliakov,*[,†] and Evgenii P. Talsi*[,†]

[†]Boreskov Institute of Catalysis, Pr. Lavrentieva 5, 630090 Novosibirsk, Russian Federation

[‡]Novosibirsk State University, Ul. Pirogova 2, 630090 Novosibirsk, Russian Federation

Supporting Information

ABSTRACT: Chiral bipyrrolidine based iron and manganese complexes $[((S,S)\text{-pdp})M^{II}(OTf)_2]$ catalyze the asymmetric epoxidation of various olefins with H_2O_2 in the presence of carboxylic acid additives with high efficiency (up to 1000 turnover number (TON)) and selectivity (up to 100%), and with good to high enantioselectivity (up to 93% enantiomeric excess (*ee*)). The enantioselectivity increases with growing steric demand of the acid. On the basis of the electron paramagnetic resonance (EPR) spectroscopy and enantioselectivity studies, the active oxygen-transferring species of the above systems can be identified as structurally similar oxometal(V) species of the type $[((S,S)\text{-pdp})M^{V}{=}O(OCOR)]^{2+}$ (M = Fe, Mn; R = alkyl).

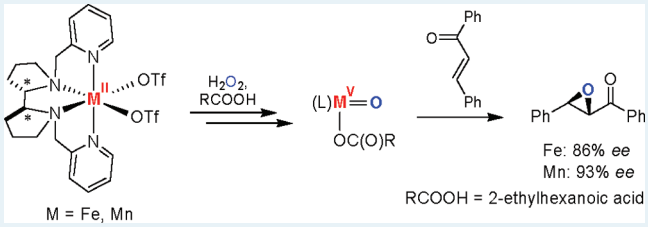

KEYWORDS: *asymmetric catalysis, epoxidation, hydrogen peroxide, intermediate, iron, manganese*

1. INTRODUCTION

The demand for efficient and sustainable regio- and stereoselective catalyst systems for the oxidation of organic substrates is continuously growing in line with toughening economic and environmental constraints. Thereby, biomimetic catalysts mimicking the reactivity of natural metalloenzymes may become a promising alternative to traditional systems in the near future. Within biomimetic oxidation catalysts, aminopyridine complexes of such biologically important elements as iron and manganese attract particular attention. To date, Fe complexes with polydentate *N*-donor ligands are regarded as the best models of natural nonheme oxygenases, capable of catalyzing selective oxidation of unactivated aliphatic C−H bonds with H_2O_2.[1−18] In a few cases, olefin epoxidations with H_2O_2 proceed stereoselectively on biomimetic Fe catalysts.[19−22] Similar Mn complexes catalyze olefin epoxidations with percarboxylic acids or H_2O_2 in a chemo- and sometimes enantioselective fashion with high efficiency.[23−31] While the nature of active species in various nonheme Fe/H_2O_2 catalyst systems has been extensively studied in the past years,[6,10,12,32−38] no mechanistic data have so far been reported for bipyrrolidine-based Fe complexes of the type **1** (Scheme 1), that are regarded as efficient and selective catalysts of C−H oxidations and asymmetric *cis*-dihydroxylations.[14,16−18] For related aminopyridine-based Mn systems, very little mechanistic data is available as yet.[24−27,29,30,39−43]

Previously, we reported that aminopyridine manganese complexes featuring chiral cyclohexanediamine and bipyrrolidine moieties are highly efficient catalysts of olefin epoxidation with H_2O_2 in the presence of acetic acid,[30] demonstrating moderate to good enantioselectivities (43−84% enantiomeric excess (*ee*)). Herein, a comparative study of asymmetric olefin epoxidation by catalyst systems $[((S,S)\text{-pdp})M^{II}(OTf)_2]/H_2O_2$/carboxylic acid (where M = Fe or Mn; Scheme 1) is reported, with focus on the effect of carboxylic acids: the use of bulkier RCOOH results in a drastic increase of enantioselectivity. The observed enantioselectivities provided a useful mechanistic information which, in combination with electron paramagnetic resonance (EPR) spectroscopy,[34,36,38] allows to reliably establish the nature of the epoxidizing species in the Fe- and Mn-based systems.

2. RESULTS AND DISCUSSION

Recently, complex **2** has been established as a highly efficient catalyst of enantioselective olefin epoxidation with H_2O_2 in the presence of acetic acid.[30] In Table 1 epoxidation results for Mn catalyst **2** and for its Fe counterpart **1**[14] are given. Optimized reaction conditions, that is, 1.1 equiv (with respect to substrate) of RCOOH for the Fe system (cf. refs 4, 16) and 14 equiv of RCOOH for the Mn system (cf. refs 27 and 30) were applied. The manganese catalyst **2** demonstrated a much higher reactivity toward the substrates used (Chart 1), that allowed the use of only 0.1 mol % of the catalyst to achieve good epoxide yields (up to 99−100%) within 2.5 h at −30 °C (Table 1). In all cases, **2** exhibited a higher enantioselectivity and efficiency than **1**. The origin of higher enantioselectivity of

Received: March 27, 2012
Revised: May 4, 2012
Published: May 8, 2012

Scheme 1. Aminopyridine Fe (1) and Mn (2) Complexes Used in This Study, and the Catalyzed Olefin Epoxidation

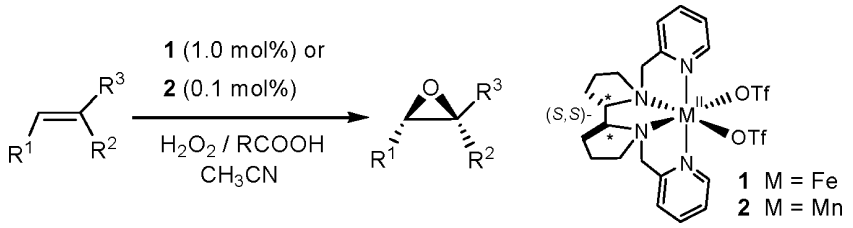

Table 1. Asymmetric Olefin Epoxidations with H_2O_2 Catalyzed by Complexes 1 and 2[a]

alkene	catalyst (mol %)	additive[b]	conversion (%)/epoxide yield (%)	*ee* (%) (config)
styrene	**1** (1.0)[c]	AA	26/26	16 (*R*)
styrene	**2** (0.1)	AA	84/84	39 (*R*)
styrene	**2** (0.1)	PA	62/62	54 (*R*)
styrene	**2** (0.1)	EHA	92/92	56 (*R*)
Z-*β*-Me-sty	**2** (0.1)	AA	63/57	45[d]
Z-*β*-Me-sty	**2** (0.1)	EHA	59/57	72[d]
p-Cl-sty	**2** (0.1)	AA	76/76	37 (*R*)
p-Cl-sty	**2** (0.1)	EHA	24/24	54 (*R*)
cy-O	**2** (0.1)	AA	61/61	55 (*R*)
cy-CN	**1** (1.0)	AA	99/99	33[d]
bna	**1** (1.0)	AA	28/28	26[d]
bna	**1** (1.0)	EHA	51/51	62[d]
bna	**2** (0.1)	AA	44/40	50[d]
bna	**2** (0.1)[e]	EHA	37/37	74[d]
bnh	**2** (0.1)	AA	76/76	52[d]
bnh	**2** (0.1)	EHA	47/47	79[d]
mcm	**2** (0.1)	AA	92/92	40 (*2R,3S*)
mcm	**2** (0.1)	EHA	37/37	77 (*2R,3S*)
dbpcn	**1** (1.0)	AA	48/48	27 (*3R,4R*)
dbpcn	**2** (0.1)	AA	74/74	76 (*3R,4R*)[f]
dbpcn	**2** (0.1)[g]	PA	77/77	90 (*3R,4R*)
dbpcn	**2** (0.1)[g]	EHA	100/100	93 (*3R,4R*)

[a]The reactions were performed at −30 °C; $[H_2O_2]/[substrate]$ = 2.0 for the Fe catalyst and $[H_2O_2]/[substrate]$ = 1.3 for the Mn catalyst; H_2O_2 was added by a syringe pump over 30 min. Conversions and epoxide yields are calculated based on the substrate. [b]For the structures and abbreviations of acidic additives see Chart 2. [c]At 0 °C, 0.55 equiv of CH_3COOH. [d]Configuration was not assigned. [e]2.0 equiv of H_2O_2 was added over 4.5 h. [f]From ref 30. [g]1.3 equiv of H_2O_2 was added over 2 h.

Chart 1. Structures, Names, or Abbreviations for Substrates Used

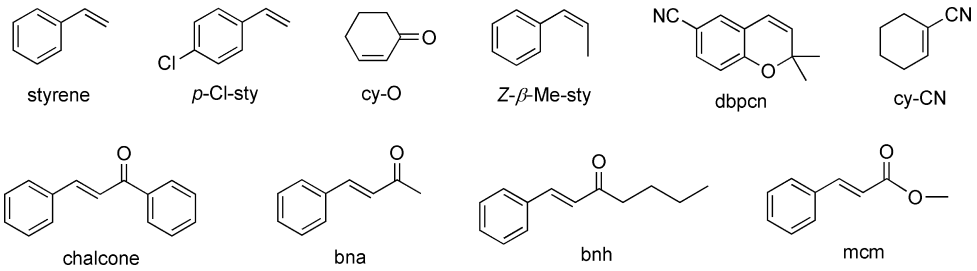

catalyst **2** is not entirely clear at the moment; however, it is not unusual that Mn systems perform better than Fe ones in enantioselective epoxidations with H_2O_2.[3] The replacement of acetic acid as additive with more sterically demanding 2-ethylhexanoic (EHA) or pivalic (PA) acid resulted in a drastic increase in enantioselectivities (+17% *ee* for dbpcn, styrene and *p*-chlorostyrene, +26% *ee* for benzylidene acetone (bna), +27% *ee* for benzylidene-2-hexanone (bnh) and for *Z*-*β*-methylstyrene, and +37% *ee* for methyl cynnamate (mcm)); in the presence of EHA, dbpcn and chalcone epoxidized with 93% *ee* (Tables 1, 2).

To probe the effect of steric bulk of the added acid on the enantioselectivity systematically, chalcone epoxidation over catalysts **1** and **2** in the absence and in the presence of eight different carboxylic acids (Chart 2) was studied (Table 2). The addition of carboxylic acid is crucial for achieving good performance of catalysts **1** and **2**: while both **1** and **2** demonstrate small (entry 1) or zero (entry 10) conversion in the absence of acid, and very small conversions in the presence of formic acid (entries 2 and 11), the use of acetic and bulkier carboxylic acids results in much higher epoxide yields and *ee*'s. The latter coincided for linear acids (entries 4−6 and 13−15):

dx.doi.org/10.1021/cs300205n | *ACS Catal.* 2012, 2, 1196−1202

Table 2. Asymmetric Epoxidation of Chalcone with H_2O_2 Catalyzed by Complexes 1 and 2: Effect of Added Carboxylic Acid[a]

entry	catalyst (mol %)	additive[b]	conversion (%)/ epoxide yield (%)	*ee* (%)[c]
1	**1** (1.0)		13/13	61
2	**1** (1.0)	FA	10/10	65
3	**1** (1.0)	AA	92/92	71
4	**1** (1.0)	BA	97/91	72
5	**1** (1.0)	VA	97/91	72
6	**1** (1.0)	CA	96/90	72
7	**1** (1.0)	IBA	97/97	78
8	**1** (1.0)	PA	100/100	84
9	**1** (1.0)	EHA	100/98	86
10	**2** (0.1)		0/–	
11	**2** (0.1)	FA	4/4	*d*
12	**2** (0.1)	AA	98/98	78[d]
13	**2** (0.1)	BA	72/69	80
14	**2** (0.1)	VA	51/48	80
15	**2** (0.1)	CA	42/40	80
16	**2** (0.1)	IBA	100/100	82[d]
17	**2** (0.1)	PA[e]	47/47	86
18	**2** (0.1)	EHA	99/97	93

[a]The reactions were performed at −30 °C; $[H_2O_2]/[substrate]$ = 2.0 for the Fe catalyst and $[H_2O_2]/[substrate]$ = 1.3 for the Mn catalyst; H_2O_2 was added by a syringe pump over 30 min. Conversions and epoxide yields are calculated based on the substrate. [b]For the structures and abbreviations of acidic additives see Chart 2. [c]Absolute configuration of chalcone epoxide was (2*R*,3*S*). [d]From ref 30. [e]3.0 equiv of H_2O_2 was added over 1 h, 21 equiv of PA was used.

Chart 2. Structures and Abbreviations for Carboxylic Acids Used

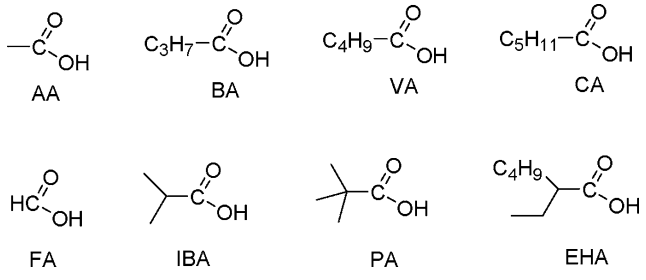

72% *ee* for **1** and 80% *ee* for **2**. For both Mn and Fe catalysts, the enantioselectivities increased in the following order: formic acid < acetic acid < *n*-butyric acid = *n*- valeric acid = *n*-caproic acid < *iso*-butyric acid < pivalic acid <2-ethylhexanoic acid, in line with rising steric demand of the carboxylic acid (Chart 2).[44]

We can conclude that (1) for both the iron and the manganese systems, the enantioselectivities increase with increasing steric bulk of the carboxylic acid additive and (2) the role of the additive is dual in that the latter assists the activation of hydrogen peroxide (and thus governs the catalytic performance) and affects the epoxidation enantioselectivity; apparently, the acid molecule is incorporated into the active species at the enantioselectivity-determining step, presumably acting as an auxiliary ligand.

What is the nature of active species responsible for the enantioselective oxygen transfer? Recently, we have successfully used EPR spectroscopy to reliably discriminate between different iron−oxygen intermediates in several nonheme iron-based catalyst systems,[34,36,38] that prompted us to use a similar approach for the systems **1**/H_2O_2 and **1**/H_2O_2/CH_3COOH.

EPR spectrum of the sample **1**/H_2O_2 = 1:2.5 frozen 1 min after the addition of H_2O_2 to the solution of **1** in a 1.7:1 CH_2Cl_2/CH_3CN mixture at −70 °C displays resonances from a low-spin (S = 1/2) iron−oxygen species **1a** (g-values in the range 1.96−2.20), and resonances in the range of g = 4.2−8 from an unidentified high-spin (S = 5/2) ferric species[45] (Figure 1A, Table 3). The increase of the $[H_2O_2]$:[**1**] ratio in

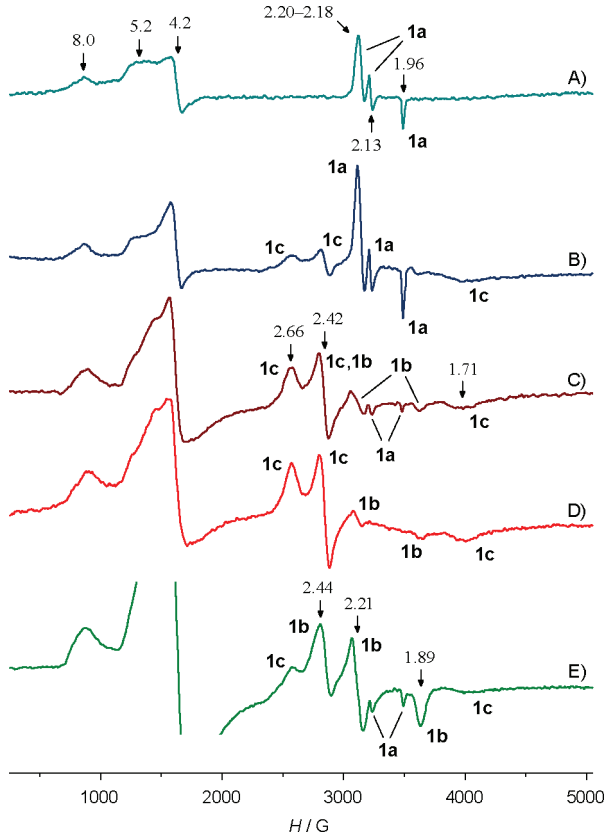

Figure 1. EPR spectra (1.7:1 CH_2Cl_2/CH_3CN, −196 °C) of samples: (A) **1**/H_2O_2 (1:2.5), (B) **1**/H_2O_2 (1:10), (C) **1**/H_2O_2/CH_3COOH (1:2.5:7.5), (D) **1**/H_2O_2/CH_3COOH (1:2.5:15), and (E) **1**/H_2O_2/CH_3COOH (1:10:10), frozen 1 min after mixing the reagents at −70 °C ([**1**] = 0.05 M).

the sample **1**/H_2O_2 results in the rise of the concentration of **1a** and in the appearance of resonances of a low-spin (S = 1/2) iron−oxygen species **1c** (Figure 1B, Table 3). The situation changes abruptly in the presence of acetic acid. The EPR spectra of the samples **1**/H_2O_2/CH_3COOH = 1:2.5:7.5 (Figure 1C), 1:2.5:15 (Figure 1D), and 1:10:10 (Figure 1E) frozen 1 min after mixing the reagents at −70 °C show predominantly resonances of **1c** and **1b**, whereas those of **1a** are very weak. Complexes **1a**−**c** are extremely unstable: **1b** and **1c** decay with half-life times of $\tau_{1/2}$ = 6 ± 2 min and 7 ± 3 min at −85 °C, respectively (Supporting Information, Figure S1), and **1a** decays with $\tau_{1/2}$ = 5 ± 1 min (−70 °C, sample **1**/H_2O_2 = 1:2.5).

It is reasonable to ascribe the resonances prevailing in the system **1**/H_2O_2 (denoted in Figure 1A as **1a**) to the superposition of the EPR spectra of the hydroperoxo complexes $[((S,S)\text{-pdp})Fe^{III}-OOH(CH_3CN)]^{2+}$ (**1a-CH$_3$CN**) and

dx.doi.org/10.1021/cs300205n | *ACS Catal.* 2012, 2, 1196−1202

Table 3. EPR Spectroscopic Data for $S = 1/2$ Iron−Oxygen Species Formed in Non-Heme Iron-Based Systems[a]

species	g_1	g_2	g_3	ref.
$[(bpmen)Fe^{III}–OOH(CH_3CN)]^{2+}$	2.218	2.175	1.966	48
$[(bpmen)Fe^{III}–OOH(H_2O)]^{2+}$	2.197	2.128	1.970	48
$[(bpmen)Fe^{III}–OH(S)]^{2+}$ [b]	2.43	2.21	1.91	48
$(bpmen)Fe^{V}=O$ [c]	2.69	2.42	1.70	34, 36
$[((S,S)\text{-pdp})Fe^{III}–OOH(CH_3CN)]^{2+}$ (**1a-CH$_3$CN**)	2.206	2.171	1.955	*e*
$[((S,S)\text{-pdp})Fe^{III}–OOH(H_2O)]^{2+}$ (**1a-H$_2$O**)	2.191	2.124	1.963	*e*
$[((S,S)\text{-pdp})Fe^{III}–OH(S)]^{2+}$ (**1b**)[b]	2.44	2.21	1.89	*e*
1c[d]	2.66	2.42	1.71	*e*

[a]EPR spectra were recorded at −196 °C. [b]S = CH_3CN or H_2O. [c]This intermediate was previously assigned to an oxoiron(V) species (refs 34, 36). [d]**1c** is assigned to the $[((S,S)\text{-pdp})Fe^{V}=O(X)]^{2+}$ complex, where X = HO^- or CH_3COO^-. [e]This work.

Scheme 2. Proposed Mechanism of Epoxidation by Non-Heme Catalyst Systems 1, $2/H_2O_2/RCOOH$

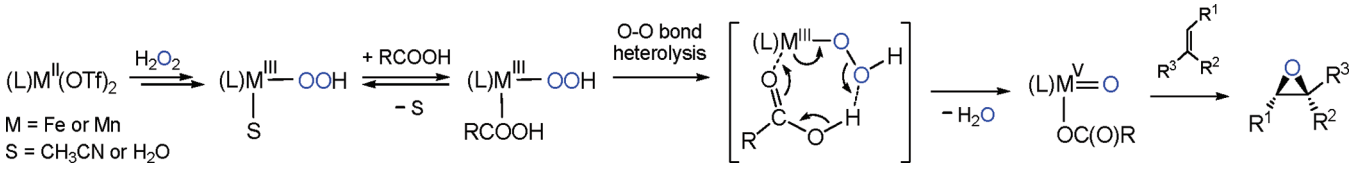

$[((S,S)\text{-pdp})Fe^{III}–OOH(H_2O)]^{2+}$ (**1a-H$_2$O**).[46] EPR parameters of **1a-CH$_3$CN** and **1a-H$_2$O** are presented in Table 3 (for simulated spectra see Supporting Information, Figure S2). In turn, the EPR spectrum of **1b** closely resembles that of $[(bpmen)Fe^{III}–OH(S)]^{2+}$ (Table 3). Hence, it is reasonable to assign **1b** to the hydroxo complex $[((S,S)\text{-pdp})Fe^{III}–OH(S)]^{2+}$ (S = CH_3CN or H_2O). The EPR spectrum of **1c** (g_1 = 2.66, g_2 = 2.42, g_3 =1.71) is very close to that of the similar intermediate observed in the system $[(bpmen)Fe^{II}(CH_3CN)_2](ClO_4)_2/H_2O_2$ (g_1 = 2.69, g_2 = 2.42, g_3 = 1.70).[34,36] Species **1a**–**1c** are less temperature-stable than related ones formed in the system $Fe(bpmen)/H_2O_2$:[34,36] in the latter case, interconversion and decay of the iron−oxygen intermediates take place at −70 to −60 °C.[47]

Earlier, using direct low-temperature reactivity studies, the decay rate of ferric hydroperoxo complexes in the $[(bpmen)Fe^{II}(CH_3CN)_2](ClO_4)_2/H_2O_2$ and related systems was shown to be unaffected by the presence of an excess of cyclohexene in the reaction solution, thus ruling out their possible key role in the catalytic oxidations.[48,49] In contrast, the decay rate of the intermediate assigned to $(bpmen)Fe^{V}=O$ (Table 3) noticeably increased in the presence of cyclohexene, and formation of cyclohexene oxide as the main reaction product was detected.[34] By analogy with the $[(bpmen)Fe^{II}(CH_3CN)_2](ClO_4)_2/H_2O_2$ system, one could expect that it is **1c** that drives the chemo- and stereoselective oxidation of olefins. The $\mathbf{1}/H_2O_2$(/CH_3COOH) catalyst system demonstrates a reactivity pattern similar to that of $[(bpmen)Fe^{II}(CH_3CN)_2](ClO_4)_2/H_2O_2$(/$CH_3COOH$). In particular, they display close catalytic behaviors toward epoxidation of cyclohexene at room temperature (Supporting Information, Table S2, entries 1–8 and 9–16). In agreement with the proposed key role of **1c** in selective epoxidations, the increase of its concentration with increasing concentration of CH_3COOH (Figure 1) correlates with the increase of cyclohexene epoxidation selectivity (Supporting Information, Table S2). The addition of 100 equiv of CH_3COOH to the $\mathbf{1}/H_2O_2$ system enhances the yield of cyclohexene epoxide, as well as the epoxidation selectivity: the latter rises from 44% to 70% in air and from 56% to 85% in argon (Supporting Information, Table S2, entries 1 and 4, and entries 5 and 8). Acetic acid additives also suppress free-radical-type side reactions (reflected by lower yields of enol and enone; see Supporting Information, Table S2 with accompanying text, and Supporting Information, Figure S4 for further details).

Enantioselectivity studies (vide supra) bear evidence in favor of similar oxygen-transferring active species in the systems $\mathbf{1}(\mathbf{2})/H_2O_2$/carboxylic acid. The elucidation of the nature of the active species **1c** detected in the Fe-based system would thus provide the key to the understanding of the nature of the active species in the Mn system as well. The enantioselectivities of chalcone epoxidation by catalyst systems $\mathbf{1}(\mathbf{2})/H_2O_2$/RCOOH depend on the nature of the carboxylic acid added (Table 2), thus indicating the presence of the carboxylic acid moiety in the active species.

Therefore, the following reaction scheme can be deduced that agrees well with our catalytic and spectroscopic observations and with literature data (Scheme 2). At the initial stage, the starting metal(II) complex is converted to the hydroperoxo-metal(III) complex $[(L)M^{III}–OOH(S)]^{2+}$. Such a species $[((S,S)\text{-pdp})Fe^{III}–OOH(S)]^{2+}$ (**1a**; S = CH_3CN or H_2O) has been identified in the system $\mathbf{1}/H_2O_2/CH_3COOH$ (Figure 1C,E). Evidence for the formation of similar $[(L')Mn^{III}–OOH]^{2+}$ species has been previously reported.[50] The hydroperoxo complex $[(L)M^{III}–OOH(S)]^{2+}$ is unlikely to epoxidize the alkene directly (vide supra and refs 48–49), but it can exchange its sixth ligand S with the carboxylic acid, followed by conversion into a reactive metal(V)-oxo complex. In this case, the presence of the carboxylic acid would facilitate the heterolysis of the O–O bond of the $[(L)M^{III}–OOH(RCOOH)]^{2+}$ intermediate.[51−53] These considerations are corroborated by the observation that increasing amount of added acetic acid results in the increase of concentration of **1c** (Figure 1); the latter could thus be assigned to the low-spin (S = 1/2) complex $[((S,S)\text{-pdp})Fe^{V}=O(OC(O)CH_3)]^{2+}$. Recently, using variable-temperature mass spectrometry, Costas, Cronin, and co-workers have trapped the active oxoiron(V) species in a related catalyst system composed of an aminopyridine iron(II) complex and hydrogen peroxide.[37] The oxoiron(V) intermediate has been found to exhibit an EPR spectrum closely resembling that of species **1c**.[38] These data provide additional support in favor of the assignment of **1c** to the oxoiron(V) active species.

dx.doi.org/10.1021/cs300205n | ACS Catal. 2012, 2, 1196–1202

It is not entirely clear at the moment why the use of formic acid as additive results in much lower yields of chalcone epoxide (Table 2, entries 2 and 11). One of possible deactivation reactions is decarboxylative degradation of the active species in the formic-acid-based systems (Supporting Information, Table S3 and Scheme S2). Additional discussion of the mechanism can be found in the Supporting Information, Table S4 (with accompanying text).

3. CONCLUSIONS

Chiral bipyrrolidine-based nonheme iron and manganese complexes **1** and **2** catalyze the enantioselective epoxidation of prochiral olefins with H_2O_2 in the presence of carboxylic acids, manganese catalyst **2** demonstrating much higher efficiency (1000 vs 100 turnover number (TON)) and enantioselectivity (up to 93% *ee*: the highest value ever reported for aminopyridine metal catalysts). The enantioselectivity rises with increasing steric bulk of the acid, thus indicating the presence of the carboxylic moiety in the active species at the enantioselectivity-determining step. On the basis of EPR and enantioselectivity data, the active species can be assigned to $[((S,S)\text{-pdp})M^{V}{=}O(OC(O)R)]^{2+}$ complexes (where M = Fe or Mn, R = alkyl). In the iron system, the corresponding intermediate $[((S,S)\text{-pdp})Fe^{V}{=}O(OC(O)CH_3)]^{2+}$ has been trapped by EPR spectroscopy at −85 °C. A consistent mechanism for the active species formation is proposed.

4. EXPERIMENTAL SECTION

Materials. All chemicals and solvents were purchased from Aldrich, Acros Organics, or Alfa Aesar and were used without additional purification unless noted otherwise. For catalytic epoxidation experiments, 30% analytical grade aqueous H_2O_2 was used. For EPR experiments, ≈ 95% H_2O_2 was obtained by distillation of commercial 30% H_2O_2 from the phosphate buffer, followed by concentration of the distillate under reduced pressure at room temperature. The exact oxidant concentrations in the prepared reagents were determined by iodometric titration under argon. Cyclohexene and styrene were purified by distillation over sodium metal. Chiral aminopyridine ligand (*S*,*S*)-pdp,[16] $Fe(OTf)_2{\cdot}2CH_3CN$,[54] $Mn(OTf)_2{\cdot}CH_3CN$,[55] complexes $[((S,S)\text{-pdp})Fe^{II}(OTf)_2]$ (**1**)[14] and $[((S,S)\text{-pdp})Mn^{II}(OTf)_2]$ (**2**)[30] were prepared as described (OTf = trifluoromethanesulfonate).

Instrumentation. ^{1}H NMR spectra of the oxidation product mixtures were measured on a Bruker DPX-250 NMR spectrometer at 250.13 MHz in 5 mm cylindrical glass tubes with the following operating conditions: spectral width 8 kHz, spectrum accumulation frequency 0.25 Hz, number of scans 32−64, radio frequency pulse 2−8 μs, 32−64k data points. Chemical shifts were internally referenced to tetramethylsilane. ^{1}H NMR spectra of the paramagnetic iron(IV)-oxo complexes were measured on a Bruker Avance 400 NMR spectrometer at 400.13 MHz in 5 mm cylindrical glass tubes with the following operating conditions: spectral width 200 kHz, spectrum accumulation frequency 5 Hz, number of scans 512−2048, radio frequency pulse 5 μs, 32k data points. Chemical shifts were referenced to the resonances of residual protons of the solvents (CD_3CN, δ = 1.96; CD_2Cl_2, δ = 5.32). EPR spectra (−196 °C) were measured in 3 mm quartz tubes on a Bruker ER-200D spectrometer at 9.3−9.4 GHz, modulation frequency 100 kHz, modulation amplitude 5 G. The dual EPR cavity furnished with the spectrometer was used. Periclase crystal (MgO) with impurities of Mn^{2+} and Cr^{3+}, which served as a side reference, was placed into the second compartment of the dual cavity. Measurements were conducted in a quartz finger Dewar filled with liquid nitrogen. EPR signals were quantified by double integration with a frozen solution of copper(II) acetylacetonate as a standard at −196 °C. EPR spectra were simulated using an extended version of the program ESR1.[56] The yields of cyclohexene oxidation products were determined using a DB-WAX capillary column [30 m × 0.25 mm ×0.25 μm, He carrier gas] on an Agilent 6890N gas chromatograph with a flame-ionization detector. Enantioselective chromatographic resolutions of epoxide enantiomers were performed on a Shimadzu LC-20 chromatograph equipped with a set of chiral columns.

Sample Preparation for EPR Measurements. Using a micropipet connected with polyethylene capillary, an appropriate amount of the oxidant in 0.05 mL of CH_3CN was added to 0.25 mL of a solution of complex **1** in a CH_2Cl_2/CH_3CN mixture at −80 to −50 °C directly in a quartz EPR tube (d = 3 mm). If necessary, acetic acid and cyclohexene were added to the solution of iron(II) complex prior to the oxidant addition. After stirring for 30−60 s with polyethylene capillary at −80 to −50 °C, the sample was frozen by immersion in liquid nitrogen, and the EPR spectrum was measured at −196 °C. For kinetic EPR studies, this sample was placed in a thermostat at required temperature directly in the EPR tube. To stop the reaction, the tube was again immersed in liquid nitrogen, followed by registration of the EPR spectrum at −196 °C. Total concentration of the low-spin (S = 1/2) species **1a**−**1c** measured by EPR did not exceed 7% of the initial concentration of **1**.

Sample Preparation for Low-Temperature NMR Measurements. Using a micropipet connected with polyethylene capillary, an appropriate amount of concentrated H_2O_2 in 0.09 mL of CD_3CN was added to 0.36 mL of a solution of complex **1** and acetic acid in a CD_2Cl_2/CD_3CN mixture at −70 °C directly in a glass NMR tube (d = 5 mm). After stirring for 1−2 min with polyethylene capillary at −70 °C, the sample was cooled by immersion in liquid nitrogen for a few seconds and immediately placed in the NMR spectrometer. For kinetic NMR measurements, NMR spectra were recorded at the same temperature.

General Procedure for Catalytic Olefin Epoxidations with H_2O_2. Iron-Catalyzed Epoxidations. Substrate (100 μmol) and the carboxylic acid (110 μmol) were added to the solution of **1** (1 μmol, 0.68 mg) in CH_3CN (400 μL), and the mixture was thermostatted at the desired temperature. Then, 100 μL of the H_2O_2 solution in CH_3CN (200 μmol of H_2O_2) was injected by a syringe pump over 30 min upon stirring (555 rpm). The resulting mixture was stirred for 2.5 h at the required temperature. The reaction was quenched with saturated aqueous solution of $NaHCO_3$, and the products were extracted with pentane (3 × 2 mL). The solvent was carefully removed in a stream of air, the residue was dissolved in 1 mL of CCl_4 and dried over $CaSO_4$. The mixture was filtered, and the filtrate was analyzed by ^{1}H NMR spectroscopy as previously described.[30] When 2-ethylhexanoic or pivalic acid additives were used, syringe pump injection of H_2O_2 was performed over 2 h.

Manganese-Catalyzed Epoxidations. Substrate (100 μmol) and the carboxylic acid (1.4 mmol) were added to the solution of **2** (0.1 μmol, 0.068 mg) in CH_3CN (400 μL), and the mixture was thermostatted at the desired temperature.

dx.doi.org/10.1021/cs300205n | ACS Catal. 2012, 2, 1196−1202

Then, 100 μL of the H_2O_2 solution in CH_3CN (130 μmol of H_2O_2) was injected by a syringe pump over 30 min upon stirring (555 rpm). The resulting mixture was stirred for 2.5 h at the required temperature. The reaction was quenched with saturated aqueous solution of $NaHCO_3$, and the products were extracted with pentane (3 × 2 mL). The solvent was carefully removed in a stream of air, the residue was dissolved in 1 mL of CCl_4 and dried over $CaSO_4$. The mixture was filtered, and the filtrate was analyzed by ^{1}H NMR spectroscopy as previously described.[30] When 2-ethylhexanoic or pivalic acid additives were used, injection of H_2O_2 was performed over 2 h.

Enantiomeric Excess Measurements. The enantiomeric excess values of cy-CN and cy-O (for abbreviations used see section Abbreviations; the structures and NMR data of the epoxides can be found in the Supporting Information) epoxides were measured by ^{1}H NMR with a chiral shift reagent Eu(hfc)$_3$ (europium tris[3-(heptafluoropropylhydroxymethylene)-(+)-camphorate]) as in ref 30. Enantioselective chromatographic resolutions of styrene, *p*-chlorostyrene, dbpcn, chalcone, bna, bnh mcm and *Z*-*β*-Me-sty epoxides (Supporting Information, Scheme S1) were performed on a Shimadzu LC-20 chromatograph using a set of chiral Diacel HPLC columns.[30] Styrene epoxide: Chiralcel OD-H column, ^{i}PrOH:*n*-hexane = 1:99, 0.6 mL/min, detection at 216 nm, t_R = 11.6 min (*S*), t_R = 12.5 min (*R*). *p*-Chlorostyrene epoxide: Chiralcel OJ-H column, ^{i}PrOH:*n*-hexane = 0.5:99.5, 1.0 mL/min, detection at 216 nm, t_R = 10.4 min (*R*), t_R = 11.4 min (*S*). Dbpcn epoxide: Chiralcel OJ-H column, ^{i}PrOH:*n*-hexane =30:70, 1.0 mL/min, detection at 254 nm, t_R = 11.0 min (3*R*,4*R*), t_R = 19.0 min (3*S*,4*S*). Chalcone epoxide: Chiralcel OD-H column, ^{i}PrOH:*n*-hexane = 2:98, 1.0 mL/min, detection at 254 nm, t_R = 17.0 min (2*S*,3*R*), t_R = 18.2 min (2*R*,3*S*). Bna epoxide: Chiralcel OB-H column, ^{i}PrOH:*n*-hexane = 5:95, 0.5 mL/min, detection at 220 nm, t_R = 39 min (minor), t_R = 48 min (major). Bnh epoxide: Chiralcel OJ-H column, ^{i}PrOH:*n*-hexane = 5:95, 1.0 mL/min, detection at 220 nm, t_R = 9.0 min (minor), t_R = 10.5 min (major). *Z*-*β*-Me-sty epoxide: Chiralcel OD-H column, ^{i}PrOH:*n*-hexane = 1:99, 0.4 mL/min, detection at 216 nm, t_R = 12.2 min (minor), t_R = 15.0 min (major). Mcm epoxide: Chiralcel OD-H column, ^{i}PrOH:*n*-hexane = 10:90, 0.8 mL/min, detection at 216 nm, t_R = 11.6 min (major), t_R = 15.5 min (minor). Experimental uncertainty of enantioselectivity measurements did not exceed ±1% *ee*.

■ ASSOCIATED CONTENT

Supporting Information

Additional experimental details, EPR spectra of the systems **1**/H_2O_2/CH_3COOH = 1:2.5:10 (Figure S1) and **1**/H_2O_2/CH_3COOH/cyclohexene = 1:2.5:10:15 (Figure S4) at −85 °C, simulated EPR spectra of hydroperoxo-iron(III) complexes **1a-CH$_3$CN** and **1a-H$_2$O**, and their superposition (Figure S2), ^{1}H NMR spectra and chemical shifts for oxoiron(IV) complexes with ligands bpmen and (*S*,*S*)-pdp (Figure S3, Table S1), additional catalytic data (Tables S2−S4), and pathway of proposed decarboxylative degradation of the active species in the formic-acid-based systems (Scheme S2). This material is available free of charge via the Internet at http://pubs.acs.org.

■ AUTHOR INFORMATION

Corresponding Author

*E-mail: bryliako@catalysis.ru (K.P.B.), talsi@catalysis.ru. (E.P.T.). Phone: +7 (383) 326 9578. Fax: +7 (383) 330 8056.

Funding

The authors thank the Russian Foundation for Basic Research, Grants 09-03-00087 and 12-03-00782, for financial support.

Notes

The authors declare no competing financial interest.

■ ACKNOWLEDGMENTS

We are grateful to Dr. Alexander Shubin for the simulation of the EPR spectra of hydroperoxo-iron(III) complexes.

■ ABBREVIATIONS

dbpcn, 2,2-Dimethyl-2H-chromene-6-carbonitrile; bna, 4-Phenyl-but-3-en-2-one; bnh, 1-phenylhept-1-en-3-one; *p*-Cl-sty, *p*-chlorostyrene; cy-O, 2-cyclohexen-1-one; Cy-CN, cyclohexen-1-carbonitrile; *Z*-*β*-Me-sty, (*Z*)-*β*-methylstyrene; mcm, methyl cinnamate (methyl (*E*)-3-phenylprop-2-enoate); EPR, electron paramagnetic resonance; AA, acetic acid; FA, formic acid; BA, *n*-butyric acid; VA, *n*-valeric acid; CA, *n*-caproic acid; IBA, *iso*-butyric acid; PA, pivalic acid; EHA, 2-ethylhexanoic acid

■ REFERENCES

(1) Costas, M.; Mehn, M. P.; Jensen, M. P.; Que, L., Jr. *Chem. Rev.* **2004**, *104*, 939−986.
(2) Sun, C.-L.; Li, B.-J.; Shi, Z.-J. *Chem. Rev.* **2011**, *111*, 1293−1314.
(3) De Faveri, G.; Ilyashenko, G.; Watkinson, M. *Chem. Soc. Rev.* **2011**, *40*, 1722−1760.
(4) White, M. C.; Doyle, A. G.; Jacobsen, E. N. *J. Am. Chem. Soc.* **2001**, *123*, 7194−7195.
(5) Costas, M.; Tipton, A. K.; Chen, K.; Jo, D.-H.; Que, L., Jr. *J. Am. Chem. Soc.* **2001**, *123*, 6722−6723.
(6) Chen, K.; Costas, M.; Kim, J.; Tipton, A. K.; Que, L., Jr. *J. Am. Chem. Soc.* **2002**, *124*, 3026−3035.
(7) Oldenburg, P. D.; Shteinman, A. A.; Que, L., Jr. *J. Am. Chem. Soc.* **2005**, *127*, 15672−15673.
(8) Oldenburg, P. D.; Que, L., Jr. *Catal. Today* **2006**, *117*, 15−21.
(9) Que, L., Jr. *Acc. Chem. Res.* **2007**, *40*, 493−500.
(10) Mas-Ballesté, R.; Que, L., Jr. *J. Am. Chem. Soc.* **2007**, *129*, 15964−15972.
(11) Company, A.; Gómez, L.; Güell, M.; Ribas, X.; Luis, J. M.; Que, L., Jr.; Costas, M. *J. Am. Chem. Soc.* **2007**, *129*, 15766−15767.
(12) Que, L., Jr.; Tolman, W. B. *Nature* **2008**, *455*, 333−340.
(13) Company, A.; Gómez, L.; Fontrodona, X.; Ribas, X.; Costas, M. *Chem.—Eur. J.* **2008**, *14*, 5727−5731.
(14) Suzuki, K.; Oldenburg, P. D.; Que, L., Jr. *Angew. Chem., Int. Ed.* **2008**, *47*, 1887−1889.
(15) Mas-Ballesté, R.; Fujita, M.; Que, L., Jr. *Dalton Trans.* **2008**, 1828−1830.
(16) Chen, M. S.; White, M. C. *Science* **2007**, *318*, 783−787.
(17) Vermeulen, N. A.; Chen, M. S.; White, M. C. *Tetrahedron* **2009**, *65*, 3078−3084.
(18) Chen, M. S.; White, M. C. *Science* **2010**, *327*, 566−571.
(19) Gelalcha, F. G.; Bitterlich, B.; Anilkumar, G.; Tse, M. K.; Beller, M. *Angew. Chem., Int. Ed.* **2007**, *46*, 7293−7296.
(20) Gelalcha, F. G.; Anilkumar, G.; Tse, M. K.; Brückner, A.; Beller, M. *Chem.—Eur. J.* **2008**, *14*, 7687−7698.
(21) Yeung, H.-L.; Sham, K.-C.; Tsang, C.-S.; Lau, T.-C.; Kwong, H.-L. *Chem. Commun.* **2008**, 3801−3803.
(22) Wu, M.; Miao, C.-X.; Wang, S.; Hu, X.; Xia, C.; Kühn, F. E.; Sun, W. *Adv. Synth. Catal.* **2011**, *353*, 3014−3022.
(23) Murphy, A.; Dubois, G.; Stack, T. D. P. *J. Am. Chem. Soc.* **2003**, *125*, 5250−5251.

(24) Nehru, K.; Kim, S. J.; Kim, I. Y.; Seo, M. S.; Kim, Y.; Kim, S.-J.; Kim, J.; Nam, W. *Chem. Commun.* **2007**, 4623−4625.
(25) Garcia-Bosch, I.; Company, A.; Fontrodona, X.; Ribas, X.; Costas, M. *Org. Lett.* **2008**, *10*, 2095−2098.
(26) Wu, M.; Wang, B.; Wang, S.; Xia, C.; Sun, W. *Org. Lett.* **2009**, *11*, 3622−3625.
(27) Garcia-Bosch, I.; Ribas, X.; Costas, M. *Adv. Synth. Catal.* **2009**, *351*, 348−352.
(28) Sham, K.-C.; Yeung, H.-L.; Yiu, S.-M.; Lau, T.-C.; Kwong, H.-L. *Dalton Trans.* **2010**, 9469−9471.
(29) Ottenbacher, R. V.; Bryliakov, K. P.; Talsi, E. P. *Inorg. Chem.* **2010**, *49*, 8620−8628.
(30) Ottenbacher, R. V.; Bryliakov, K. P.; Talsi, E. P. *Adv. Synth. Catal.* **2011**, *353*, 885−889.
(31) Garcia-Bosch, I.; Gómez, L.; Polo, A.; Ribas, X.; Costas, M. *Adv. Synth. Catal.* **2012**, *354*, 65−70.
(32) Yoon, J.; Wilson, S. A.; Jang, Y. K.; Seo, M. S.; Nehru, K.; Hedman, B.; Hodgson, K. O.; Bill, E.; Solomon, E. I.; Nam, W. *Angew. Chem., Int. Ed.* **2009**, *48*, 1257−1260.
(33) Company, A.; Feng, Y.; Güell, M.; Ribas, X.; Luis, J. M.; Que, L., Jr.; Costas, M. *Chem.—Eur. J.* **2009**, *15*, 3359−3362.
(34) Lyakin, O. Y.; Bryliakov, K. P.; Britovsek, G. J. P.; Talsi, E. P. *J. Am. Chem. Soc.* **2009**, *131*, 10798−10799.
(35) Das, P.; Que, L., Jr. *Inorg. Chem.* **2010**, *49*, 9479−9485.
(36) Lyakin, O. Y.; Bryliakov, K. P.; Talsi, E. P. *Inorg. Chem.* **2011**, *50*, 5526−5538.
(37) Prat, I.; Mathieson, J. S.; Güell, M.; Ribas, X.; Luis, J. M.; Cronin, L.; Costas, M. *Nat. Chem.* **2011**, *3*, 788−793.
(38) Lyakin, O. Y.; Prat, I.; Bryliakov, K. P.; Costas, M.; Talsi, E. P. *Inorg. Chem.*, submitted for publication.
(39) In a Mn-Me_3tacn/H_2O_2 based system, formation of oxomanganese(V) active species was evidenced by ESI-MS, see refs 40−43.
(40) Gilbert, B. C.; Kamp, N. W. J.; Lindsay Smith, J. R.; Oakes, J. *J. Chem. Soc., Perkin Trans. 2* **1998**, 1841−1844.
(41) Gilbert, B. C.; Lindsay Smith, J. R.; Mairata i Payeras, A.; Oakes, J.; Pons i Prat, R. *J. Mol. Catal. A: Chem.* **2004**, *219*, 265−272.
(42) Gilbert, B. C.; Lindsay Smith, J. R.; Mairata i Payeras, A.; Oakes, J. *Org. Biomol. Chem. 2* **2004**, 1176−1180.
(43) Lindsay Smith, J. R.; Gilbert, B. C.; Mairata i Payeras, A.; Murray, J.; Lowdon, T. R.; Oakes, J.; Pons i Prat, R.; Walton, P. H. *J. Mol. Catal. A: Chem.* **2006**, *251*, 114−122.
(44) Another crucial parameter is the strength of the acid: Parthasarathi, R.; Padmanabhan, J.; Elango, M.; Chitra, K.; Subramanian, V.; Chattaraj, P. K. *J. Phys. Chem. A* **2006**, *110*, 6540−6544. While acids used in Table 2 had $pK_a \geq 3.55$, catalytic experiments with a stronger chloroacetic acid ($pK_a = 2.87$) resulted in 2% and 0% conversions for catalysts **1** and **2**, respectively, and trifluoroacetic acid ($pK_a = 0.63$) gave zero conversion with **2**.
(45) Analysis of EPR spectra of the catalyst systems $[LFe^{II}]^{2+}/H_2O_2$, where L = tpa, bpmen, and *S,S*-pdp, shows that resonance at $g = 4.3$ is observed in all these systems. Its intensity increases at the initial stage of reaction onset at low temperature and then drops to a constant value. In the case of tpa based system, the maximum intensity of the resonance at $g = 4.3$ is 10 times smaller than in the case of bpmen and *S,S*-pdp based complexes. Most plausibly, the resonance at $g = 4.3$ corresponds to a superposition of signals of high-spin ferric hydroperoxo and hydroxo species, and of some products of the catalyst degradation. At the initial stage of the reactions, mainly high-spin ferric hydroperoxo and hydroxo species contribute to the resonance at $g = 4.3$. Then, those complexes decay, and the residual resonance at $g = 4.3$ mainly reflects the presence of relatively stable products of catalyst degradation.
(46) The EPR spectrum very similar to that of **1a** was previously observed in $[(bpmen)Fe^{II}(CH_3CN)_2](ClO_4)_2/H_2O_2$ system, and found to belong to the superposition of the spectra of complexes $[(bpmen)Fe^{III}-OOH(CH_3CN)]^{2+}$ and $[(bpmen)Fe^{III}-OOH(H_2O)]^{2+}$ (Table 3).[36]
(47) Formation of catalytically inactive Fe^{IV}=O species was detected by ^{1}H NMR at higher temperatures (−70 °C). For details see Table S1 with accompanying text, and Figure S3 in the Supporting Information.
(48) Duban, E. A.; Bryliakov, K. P.; Talsi, E. P. *Mendeleev Commun.* **2005**, *15*, 12−14.
(49) Park, M. J.; Lee, J.; Suh, Y.; Kim, J.; Nam, W. *J. Am. Chem. Soc.* **2006**, *128*, 2630−2634.
(50) Groni, S.; Dorlet, P.; Blain, G.; Bourcier, S.; Guillot, R.; Anxolabéhère-Mallart, E. *Inorg. Chem.* **2008**, *47*, 3166−3172.
(51) Cf. the so-called "carboxylic acid-assisted" mechanism recently proposed by Que and Rybak-Akimova with co-workers.[10,12,35,52,53]
(52) Makhlynets, O. V.; Rybak-Akimova, E. V. *Chem.—Eur. J.* **2010**, *16*, 13995−14006.
(53) Makhlynets, O. V.; Das, P.; Taktak, S.; Flook, M.; Mas-Ballesté, R.; Rybak-Akimova, E. V.; Que, L., Jr. *Chem.—Eur. J.* **2009**, *15*, 13171−13180.
(54) Hagen, K. S. *Inorg. Chem.* **2000**, *39*, 5867−5869.
(55) Bryan, P. S.; Dabrowiak, J. C. *Inorg. Chem.* **1975**, *14*, 296−299.
(56) Shubin, A. A.; Zhidomirov, G. M. *J. Struct. Chem.* **1989**, *30*, 414−417.